NASA/TM—2015-218835

AIAA–2015–1101

Comparison of Numerically Simulated and Experimentally Measured Performance of a Rotating Detonation Engine

Daniel E. Paxson
Glenn Research Center, Cleveland, Ohio

Matthew L. Fotia and John Hoke
Innovative Scientific Solutions Inc., Dayton, Ohio

Fred Schauer
U.S. Air Force Research Laboratory, Wright-Patterson AFB, Ohio

August 2015

NASA STI Program . . . in Profile

Since its founding, NASA has been dedicated to the advancement of aeronautics and space science. The NASA Scientific and Technical Information (STI) Program plays a key part in helping NASA maintain this important role.

The NASA STI Program operates under the auspices of the Agency Chief Information Officer. It collects, organizes, provides for archiving, and disseminates NASA's STI. The NASA STI Program provides access to the NASA Technical Report Server—Registered (NTRS Reg) and NASA Technical Report Server—Public (NTRS) thus providing one of the largest collections of aeronautical and space science STI in the world. Results are published in both non-NASA channels and by NASA in the NASA STI Report Series, which includes the following report types:

- TECHNICAL PUBLICATION. Reports of completed research or a major significant phase of research that present the results of NASA programs and include extensive data or theoretical analysis. Includes compilations of significant scientific and technical data and information deemed to be of continuing reference value. NASA counter-part of peer-reviewed formal professional papers, but has less stringent limitations on manuscript length and extent of graphic presentations.

- TECHNICAL MEMORANDUM. Scientific and technical findings that are preliminary or of specialized interest, e.g., "quick-release" reports, working papers, and bibliographies that contain minimal annotation. Does not contain extensive analysis.

- CONTRACTOR REPORT. Scientific and technical findings by NASA-sponsored contractors and grantees.

- CONFERENCE PUBLICATION. Collected papers from scientific and technical conferences, symposia, seminars, or other meetings sponsored or co-sponsored by NASA.

- SPECIAL PUBLICATION. Scientific, technical, or historical information from NASA programs, projects, and missions, often concerned with subjects having substantial public interest.

- TECHNICAL TRANSLATION. English-language translations of foreign scientific and technical material pertinent to NASA's mission.

For more information about the NASA STI program, see the following:

- Access the NASA STI program home page at http://www.sti.nasa.gov

- E-mail your question to help@sti.nasa.gov

- Fax your question to the NASA STI Information Desk at 757-864-6500

- Telephone the NASA STI Information Desk at 757-864-9658

- Write to:
  NASA STI Program
  Mail Stop 148
  NASA Langley Research Center
  Hampton, VA 23681-2199

NASA/TM—2015-218835 AIAA–2015–1101

Comparison of Numerically Simulated and Experimentally Measured Performance of a Rotating Detonation Engine

Daniel E. Paxson
Glenn Research Center, Cleveland, Ohio

Matthew L. Fotia and John Hoke
Innovative Scientific Solutions Inc., Dayton, Ohio

Fred Schauer
U.S. Air Force Research Laboratory, Wright-Patterson AFB, Ohio

Prepared for
SciTech 2015
sponsored by the American Institute of Aeronautics and Astronautics
Kissimmee, Florida, January 5–9, 2015

National Aeronautics and
Space Administration

Glenn Research Center
Cleveland, Ohio 44135

August 2015

This report is a formal draft or working paper, intended to solicit comments and ideas from a technical peer group.

This report contains preliminary findings, subject to revision as analysis proceeds.

Level of Review: This material has been technically reviewed by technical management.

Available from

NASA STI Program
Mail Stop 148
NASA Langley Research Center
Hampton, VA 23681-2199

National Technical Information Service
5285 Port Royal Road
Springfield, VA 22161
703-605-6000

This report is available in electronic form at http://www.sti.nasa.gov/ and http://ntrs.nasa.gov/

Comparison of Numerically Simulated and Experimentally Measured Performance of a Rotating Detonation Engine

Daniel E. Paxson
National Aeronautics and Space Administration
Glenn Research Center
Cleveland, Ohio 44130

Matthew L. Fotia and John Hoke
Innovative Scientific Solutions Inc.
Dayton, Ohio 45440

Fred Schauer
U.S. Air Force Research Laboratory
Wright-Patterson AFB, Ohio 45433

Abstract

A quasi-two-dimensional, computational fluid dynamic (CFD) simulation of a rotating detonation engine (RDE) is described. The simulation operates in the detonation frame of reference and utilizes a relatively coarse grid such that only the essential primary flow field structure is captured. This construction and other simplifications yield rapidly converging, steady solutions. Viscous effects, and heat transfer effects are modeled using source terms. The effects of potential inlet flow reversals are modeled using boundary conditions. Results from the simulation are compared to measured data from an experimental RDE rig with a converging-diverging nozzle added. The comparison is favorable for the two operating points examined. The utility of the code as a performance optimization tool and a diagnostic tool are discussed.

Nomenclature

a	nondimensional speed of sound
a^*	reference speed of sound, 1250 ft/s
f	air to fuel ratio (by mass)
g_c	Newton constant, 32.174 ft-lb_m/lb_f/s^2
h	nondimensional annulus height
h_f	fuel heating value, 51,571 Btu/lb_m
l	circumferential length
p	nondimensional pressure
p_{man}	nondimensional inlet manifold total pressure
p^*	reference pressure, 14.7 psia
q_0	nondimensional heat addition parameter
t	nondimensional time
u	nondimensional circumferential velocity
u_{det}	nondimensional detonation circumferential velocity
v	nondimensional axial velocity
$\underline{w}$	conserved variables vector
x	nondimensional circumferential distance
y	nondimensional axial distance
z	reactant fraction
$\underline{F}$	circumferential flux vector
$\underline{G}$	axial flux vector
K_0	nondimensional reaction rate constant
R_g	mixture gas constant, 73.92 ft-lb_f/lb_m/R
$\underline{S}$	source term vector
T	nondimensional temperature
T^*	reference temperature, 520 R
T_{c0}	nondimensional reaction temperature
T_{man}	nondimensional manifold temperature
ε	ratio of inlet injector area to RDE annulus area at the inlet end
ϕ	equivalence ratio
γ	mixture ratio of specific heats, 1.264
ρ	nondimensional density
ρ^*	reference density, 0.055 lb_m/ft^3

1.0 Introduction

The rotating detonation engine (RDE) represents an intriguing approach to achieving pressure gain combustion (PGC) for propulsion and power systems. The RDE essentially consists of an annulus with one end open (or having a nozzle) and the other end having a one-way inlet (i.e., mechanically or aerodynamically valved). Fuel and oxidizer enter axially through the inlet end. The detonation travels circumferentially, pressurizing and heating the majority of the flow that has entered. The flow then expands, accelerates, and exits,

predominantly axially, through the open end. The exiting flow is at a higher average total pressure than the entering flow and can in principle produce more thrust (with a nozzle) or work (with a turbine) than a conventional so-called constant pressure combustion process. An illustration of a basic RDE cycle can be seen in Figure 1 which shows computed contours of temperature throughout the 'unwrapped' annular region at a moment in time.

The potential advantages of this approach compared to conventional pulsed detonation engines (PDE's) include the elimination of initiation and deflagration to detonation transition (DDT) devices, exceptionally high cycle rates (on the order of 10^3 Hz.) governed by the transit time of the detonation around the circumference, and extremely compact design options.

Although these devices have been demonstrated in the laboratory (Refs. 1 to 5), until recently there have been very few built that have been instrumented sufficiently to measure performance or to compare with modeling efforts. Meanwhile, most published modeling efforts have been focused on somewhat idealized systems, as there has been very little data available on which to tune and test loss models (Refs. 6 to 9).

This paper represents an initial attempt at bridging this gap wherein results from a computational fluid dynamic (CFD) model with loss sub-models are compared to measurements from an instrumented RDE having a converging-diverging exhaust nozzle. A simplified, two-dimensional, CFD model has been developed which operates in the reference frame of the rotating detonation and is therefore steady when converged (Ref. 6). It is largely idealized with the exception of a loss model to account for the effects of typical RDE inlets which generally consist of a throat having considerably smaller cross sectional area than the RDE annulus. For the present work, axial annulus area variation capability has been added (i.e., it is quasi-two-dimensional, or Q-2-D), along with loss sub-models to account for viscous and heat transfer effects between walls and working fluid. A loss sub-model has also been added to assess the impact of potential flow reversal at the inlet end caused by the high pressure spike behind the detonation. Since present RDE's do not have mechanical inlet valves this is a distinct possibility depending upon the manifold pressure with which the RDE is fed and the size of the aforementioned inlet throat. The added sub-models are directly adapted from validated quasi-one-dimensional models used in PDE simulations (Refs. 10 to 13). As such, only brief descriptions will be provided here. Details of the Q-2-D formulation for the governing equations will be provided.

The RDE experiment has been described in Reference 14. Therefore, only relevant details will be presented in this paper. The simulation will be compared to the experiment at two operating points. Comparison will be based on thrust, mass flow rate, and pressure at several axial locations.

It will be shown that the simulation and experiment compare quite favorably, and that the simulation can therefore be used to assess the performance impact of various RDE design and flow features.

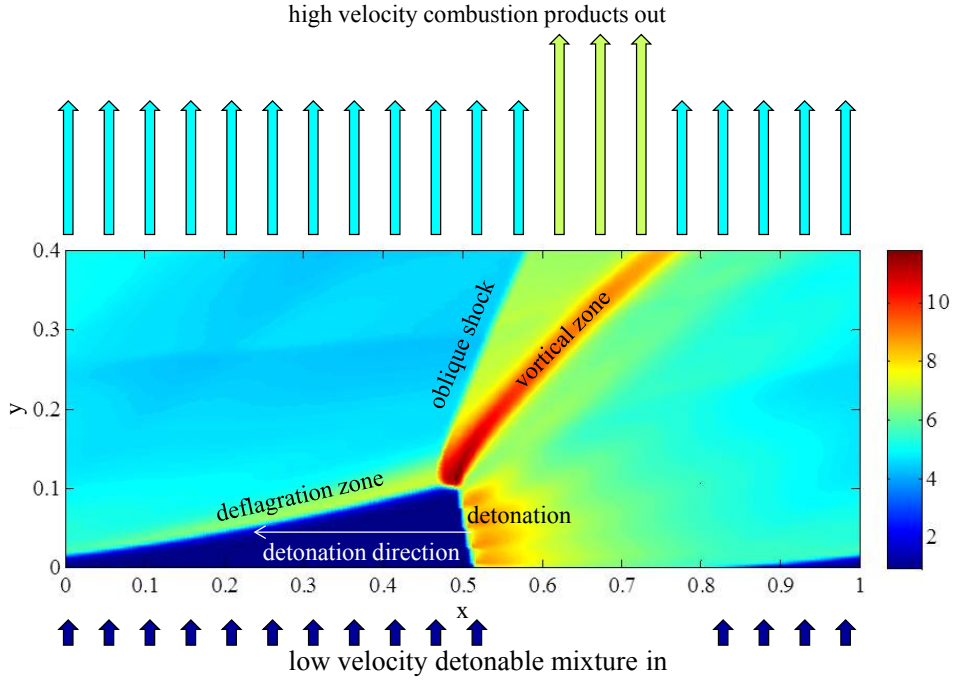

Figure 1.—Computed contours of nondimensional temperature throughout the annulus of an 'unwrapped', idealized RDE, at a moment in time during the cycle.

2.0 Simulation Description

2.1 Governing Equations

On the assumptions that the annulus radius of curvature is much greater than the height, and that the working fluid is a calorically perfect gas, the governing equations of motion may be written in nondimensional, detonation frame of reference form as follows.

$$\frac{\partial h\underline{w}}{\partial t}+\frac{\partial h\underline{F}}{\partial x}+\frac{\partial h\underline{G}}{\partial y}=\underline{S} \tag{1}$$

where

$$\underline{w}=\begin{bmatrix} \rho h \\ \rho u h \\ \rho v h \\ \dfrac{ph}{\gamma(\gamma-1)}+\dfrac{\rho\left(u^2+v^2\right)h}{2} \\ \rho z h \end{bmatrix} \tag{2}$$

$$\underline{F}=\begin{bmatrix} \rho u h \\ \left(\dfrac{p}{\gamma}+\rho u^2\right)h \\ \rho u v h \\ u\left(\dfrac{p}{(\gamma-1)}+\dfrac{\rho\left(u^2+v^2\right)}{2}\right)h \\ \rho u z h \end{bmatrix} \tag{3}$$

$$\underline{G}=\begin{bmatrix} \rho v h \\ \rho u v h \\ \left(\dfrac{p}{\gamma}+\rho v^2\right)h \\ v\left(\dfrac{p}{(\gamma-1)}+\dfrac{\rho\left(u^2+v^2\right)}{2}\right)h \\ \rho v z h \end{bmatrix} \tag{4}$$

$$\underline{S}=\begin{bmatrix} 0 \\ -c_f\left(\rho|u-u_{\det}|\right)^{0.8}\left(u-u_{\det}\right) \\ \dfrac{p}{\gamma}\dfrac{dh}{dy}-c_f\left(\rho|v|\right)^{0.8}v \\ \rho z q_0\begin{Bmatrix} K_0;T>T_{c0} \\ 0;T\le T_{c0}\end{Bmatrix}h+h_f\left(\rho\sqrt{\left(u-u_{\det}\right)^2+v^2}\right)^{0.8}\left(T_{wall}-T\right) \\ -\rho z\begin{Bmatrix} K_0;T>T_{c0} \\ 0;T\le T_{c0}\end{Bmatrix}h \end{bmatrix} \tag{5}$$

The governing equations are closed with the equation of state, which is written as follows.

$$p=\rho T \tag{6}$$

The nondimensional pressure, p, density, ρ, temperature, T, and velocities, u and v have been obtained using a reference state p^*, ρ^*, T^* and the corresponding sound speed a^*. The nondimensional distances, x and y have been obtained using the circumference, l. The nondimensional time, t has been scaled using the nominal circumferential wave transit time, l/a^*. The nondimensional annulus height, h, represents the cross-sectional area normalized by a reference area. The source term vector, Equation (5) contains expressions to account for wall friction, area variation, heat transfer, heat release and reaction rate. The constants c_f and h_f are correlated friction and heat transfer coefficients that depend on fluid properties and geometry (Ref. 13). The wall temperature T_{wall} is assumed to be room temperature since all of the experiments simulated in this paper were run for very short periods of time (on the order of 1 sec.).

The finite rate reaction model in Equation (5) is a very simple one which simply states that the reaction rate is equal to the product of a rate constant, K_0, and the amount of reactant present. However, the reaction is not allowed to proceed unless the reactants are above a reaction temperature, T_{c0}. The heat of reaction of the reactant gas mixture, q_0 is a constant which depends on the assumed fuel, oxidizer, and air-to-fuel ratio corresponding to the reactant fraction, $z = 1.0$.

$$q_0=\frac{h_f}{\gamma R_g T^*(f+1)} \tag{7}$$

For the remainder of the paper, all quantities displayed or discussed are considered nondimensional unless stated explicitly otherwise.

2.2 Numerical Treatment

The governing equations are integrated numerically in time using an explicit, second-order, two-step, Runge-Kutta technique. Spatial flux derivatives are approximated as flux differences, with the fluxes at the discrete cell faces evaluated using Roe's approximate Riemann solver. Second-order spatial accuracy (away from discontinuities) is obtained using piecewise linear representation of the primitive variable states within the cells (MUSCL). Oscillatory behavior is avoided by limiting the linear slopes. More details of the method may be found in Reference 6, which also demonstrates limited numerical validation.

2.3 Boundary Conditions

Referring to Figure 1, the following boundary conditions are imposed. At x=0.0 and x=1.0, periodic (aka symmetric) conditions are used. This means the rightmost boundary image cells are assigned the value of the leftmost interior cells at each y location. Similarly the leftmost boundary image cells are assigned the value of the rightmost interior cells. The symmetry boundary insures that the x-dimension of the computational space faithfully represents an annulus (which is continuous and has no boundary). At $y = y_{max}$, constant pressure outflow is used along with characteristic equations to obtain ρ, and v for the image cells. If the resulting flow is sonic, or supersonic, then the imposed pressure is disregarded. If, in addition, the upstream flow is supersonic, then p, ρ, and v are extrapolated from the interior (Ref. 10). The possibility for a normal shock solution whereby supersonic outflow jumps to subsonic is also accommodated. The x-velocity component u is set equal to the last interior cell at each location.

At y = 0.0 (the inflow face), partially open boundary conditions are applied as described and validated in Reference 11. This face is presumably fed by a large manifold at a fixed total pressure, and temperature. The manifold terminates at the face and is separated from it via an orifice. The ratio of orifice flow area to RDE annulus area, ε is generally less than 1. If the interior pressure is less than the manifold pressure, p_{man}, then inflow occurs. The boundary condition routine determines p, ρ, and v for the inflow face image cells subject to a momentum (total pressure) loss model which depends on the mass flow rate and the value of ε. It is capable of accommodating a scenario where the orifice becomes choked. The x-velocity component u is prescribed during inflow, and it is here that a reference frame change is implemented. Rather than specify u=0 (i.e., no swirl) which is the laboratory or fixed frame condition, the negative of the detonation speed, u_{det} is prescribed instead. As a result of this change to the detonation reference frame, the computational space becomes one where a steady-state solution is possible. If the interior pressure along the inlet face is greater than p_{man}, as might be found just behind the detonation, then there will be backflow into the manifold through the orifice. The boundary condition routine can accommodate this as well. Based on the aerodynamic shaping of the upstream side of the experimental inlet orifice, and the nonaerodynamic shape of the downstream side, an effective area (equivalent to a discharge coefficient) of 60 percent of the prescribed orifice area is used in backflow regions (Ref. 15).

In RDE simulations where inlet backflow occurs, the total mass and enthalpy that flow backward are averaged over the circumferential backflow span (recalling that in the steady detonation frame of reference, time is simply span divided by detonation velocity). When the interior pressure subsequently drops below p_{man} and forward flow resumes, all of the mass that flowed backward is sent back into the RDE at the same average enthalpy that it exited. Once this mass has re-entered, the prescribed manifold premixed air and fuel mixture enthalpy is used.

Although the model assumes that premixed air and fuel enter through the inlet, the reality of most RDE experiments is that fuel and air are injected separately. The dynamics and feed pressures of the two injection systems can be quite different, particularly during lean operation. This raises the possibility that as the rotating detonation passes a given point, it may stop or even reverse the flow in both injectors; however, the resumption of inflow may occur at different times in each. This, in turn, may raise the possibility of a purging period where air enters the RDE for part of the cycle without having fuel added to it. In order to crudely explore the effects of this possibility, the prescribed inlet reactant fraction of the model may be set to zero over various portions of the circumference. This will be utilized in the results section of the paper.

2.4 Solution Procedure

The prescribed detonation speed is not known a priori. It must be found iteratively. An initial guess is made for u_{det} and the simulation is run for the amount of time corresponding to three annular revolutions of the detonation. The domain is then examined to determine if the detonation has migrated from its initial position. If it has moved to the right of where it started, then the initial guess at u_{det} is too high. If the detonation front has moved to the left, then the initial guess is too low. Based on these results, a new guess is made for u_{det}, and the simulation is run for another 3 cycles. The process continues until the detonation front remains stationary and the entire domain stops changing. As described in Reference 6, the simulation deliberately uses a very course grid. For the simulations in this paper, a maximum of approximately 25,000 grid points define

the domain. This fact, combined with other simplifications (e.g., a one species reaction equation) mean that each iteration takes on the order of one minute on a laptop computer.

The process of initializing the simulation such that the flowfield contains a detonation on which speed iterations can be made is outlined in Reference 6.

2.5 Deflagration and Detonation Zones

As illustrated in Figure 1, the primary heat release mechanism in an RDE is a detonation. However, there is also a region where deflagration can occur. This is because fresh charge (fuel and air) is introduced to the RDE adjacent to hot combustion products. If the flow field, and numerical approximation thereof, were truly inviscid, no reaction would occur in this region. In real flows however, there is always diffusion; and the best CFD schemes cannot completely avoid numerical diffusion even when physical diffusion terms are neglected. Diffusion results in combustion products heating the premixed charge, thereby allowing the chemical reaction to proceed.

The particularly simple reaction mechanism used in the present model, together with the coarse grid which generates relatively high numerical diffusion, can lead to unrealistically high flame speeds in the deflagration zone. In order to control this, the reaction rate constant, K_0 is reduced in specified regions of the computational space as detailed in Reference 6. Briefly, and with reference to Figure 1, the regions of low K_0 are two rectangles defined as $0.00 \le y \le 0.10,\ 0 \le x \le 0.48$ and $0.00 \le y \le 0.10,\ 0.60 \le x \le 1.00$. The fraction of the incoming flow which deflagrates rather than detonates has an impact on RDE performance. To date however, it has not been possible to experimentally determine what this fraction is. For most of the simulations shown in this paper, rate parameters were set so that approximately 8 percent of the flow deflagrates. The impact of other deflagration fractions will be briefly discussed in the discussion section.

3.0 Experiment Description

A detailed description of the experimental setup may be found in Reference 14. In brief, the annular, axisymmetric rig is shown schematically and to scale in Figure 2. The profile shown in blue represents the actual RDE shape. The profile in black is the Q-2-D equivalent (i.e., same annulus area, and effective hydraulic diameter, but fixed mean radius). The rig is 21.86 in. long, with a mean diameter at the RDE annulus of 5.76 in. Air and fuel (H_2) are injected separately through manifolds that feed orifices of known size. Each manifold is fed by a calibrated choked flow orifice supplied at a very high pressure. During operation therefore the mass flow rate of fuel and air into the manifolds are constant and known. The mass flow rates of fuel and air into the RDE are highly unsteady (though periodic). However, once the manifold pressures, which are measured, become steady on a cycle-averaged basis, this setup insures that the time average mass flow rates into the RDE are identical to the constant mass flow rates into the manifolds. It is noted here that the simulation described above assumes a premixed flow entering the RDE through a single slit orifice. As such, the inlet orifice area used in the simulation is comparable to the combined areas of the experimental fuel and air orifices. The fluid properties used in the simulation are based on a stoichiometric mixture of air and hydrogen.

The rig has a series of static pressure taps placed at the locations shown in Figure 2. The taps are connected to 3 ft long tubes of 0.023 in. inner diameter, terminated with a pressure transducer. The long narrow tube damps the cyclic pressure oscillations and thermally protects the transducer. The arrangement has been given the name capillary tube averaged pressure (CTAP) and is thought to provide a close approximation to a time average (Ref. 16). The entire rig is mounted on a thrust stand such that gross thrust can be measured at any operating point. It is operated in an open air facility, so the exit pressure is atmospheric.

Figure 3 shows the nondimensional cross-sectional area of the rig (referenced to the area at the inlet end) as a function of the axial distance. The actual cross-section is shown, as is the smooth approximation (i.e., having a continuous first

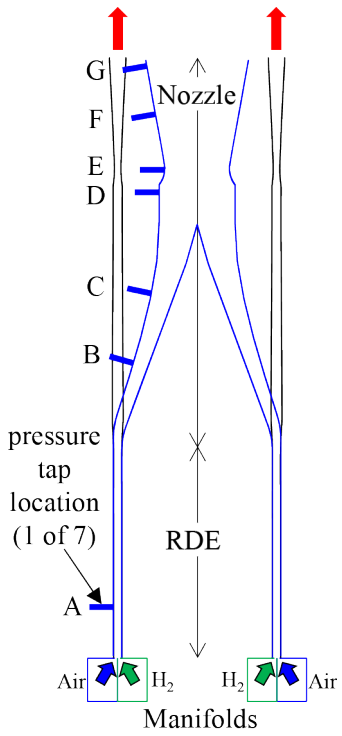

Figure 2.—Experimental RDE rig schematic.

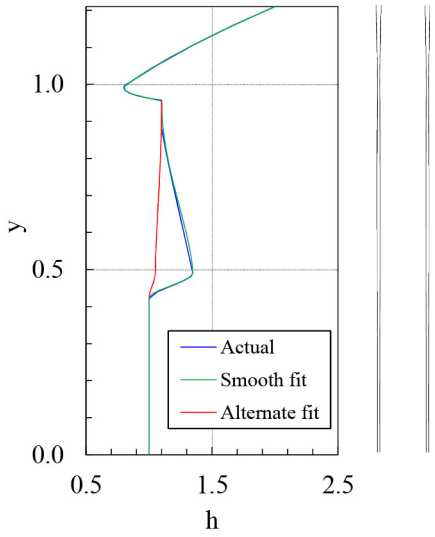

Figure 3.—Cross sectional area profile as a function of normalized axial distance. Dashed red profiles represent potential 'effective' profile caused by flow separation.

TABLE 1.—TEST POINT PARAMETERS

Test point	ϕ	Total mass flow rate, lb_m/s	T_{man}	p_{man}	Thrust, lb_f
1	1.0	4.22	1.0	35.99	620.3
2	0.42	3.95	1.0	34.29	388.0

derivative) used in the simulation. With this view, it is clear that at $y = 0.42$ there is a rapid increase in area. As will be discussed in the next section, the data indicates flow separation in this area. In order to test that possibility, the alternate profile shown in Figure 3 was implemented in the simulation. This profile represents a notional streamline of the main flow created by the separated and recirculating flow.

4.0 Results

Two operating points were compared representing stoichiometric, and lean operation. Relevant quantities are shown in Table 1. The simulated inlet manifold pressure and temperature were set to match the experimental air manifold conditions. These high feed pressures result in very little backflow through the air injector. The mixture heating value q_0 corresponds to stoichiometric hydrogen and air. The ratio of specific heats used is $\gamma = 1.264$. Dimensional reference conditions are $T^* = 520$ R, $p^* = 14.7$ psia, $\rho^* = 0.055$ lb_m/ft^3, $a^* = 1250$ ft/s. The inlet orifice-to-annulus area ratio, ε was adjusted until the

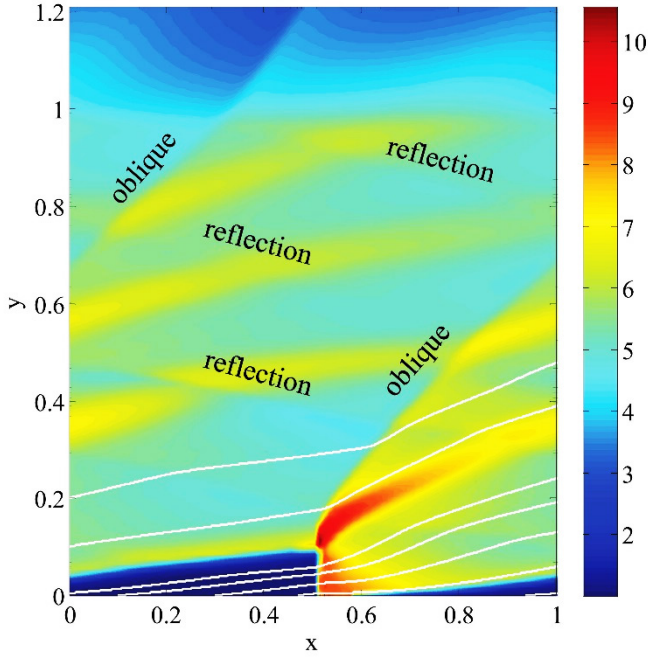

Figure 4.—Computed contours of temperature throughout the annulus of the experimental RDE at the Test Point 1 flow conditions.

simulated mass flow rate matched the measured value to within 1 percent. The simulation was then compared to the experiment on the basis of: required vs. actual ε (0.079), thrust, detonation speed (where available) and CTAP distribution.

4.1 Test Point 1: Stoichiometric ($\phi = 1.0$)

The converged flow field solution for Test Point 1, using the original smooth fit to the RDE profile of Figure 3, is shown in Figure 4. The same temperature contour format used for Figure 1 is used here. Also shown in the figure are several streamlines (in white) indicating the path of select particles from where they enter the domain until they reach the right hand side (in the detonation reference frame). All of the characteristic features of Figure 1 are seen in Figure 4. Additionally, the presence of a throat near the exit causes the majority of the upstream flow to be subsonic such that the oblique shock generated by the detonation is reflected from the throat and travels back upstream. The reflection is just visible and labelled in Figure 4. The required value of ε to match the mass flow rate was just 5 percent above the actual value. The value of u_{det} required to achieve a steady solution was 14 percent below the theoretical Chapman-Jouguet (CJ) velocity for a classical 1-D detonation. This compares favorably with measured values which are often 20 percent below the CJ value as reported in Reference 14. The computed gross thrust was only 1 percent below the measured value.

Figure 5 shows the computed axial distribution of time-averaged dimensional pressure (recall that a circumferential space average is identical to a time-average in this frame of reference) and compares it to experimental measurements made using CTAP's. The match is remarkably good with the exceptions of points A, and to lesser degrees, points B & C. The point A disparity may be due to a mixing delay which causes a downstream axial shift of the detonation. This will be discussed later. Also shown in the figure is the time-averaged pressure distribution computed using the alternate, separation-induced area profile of Figure 3. Temperature contours for this solution are not shown as they are indistinguishable from Figure 4. Other computed results were also nearly the same: ε was 4 percent above actual; thrust was 2 percent below measured. However, it is seen that the match to the CTAP data in the vicinity of the proposed separation region (near B &C) is much better. While this result does not prove that separation is occurring, it does lend credence to the possibility. As such, for the remainder of the paper, the alternate profile will be utilized in all simulation results.

Of the two test points examined, this was the only one to computationally exhibit the inlet backflow scenario described earlier. This is shown in Figure 6 where the inlet mass flux is plotted as a function of circumferential distance. With reference to Figure 4, it can be seen that the backflow occurs just behind the detonation front. The total mass that flows backward is only 0.6 percent of the total inflow, so the impact is minimal. For other RDE experiments with lower manifold pressures, this may not be the case.

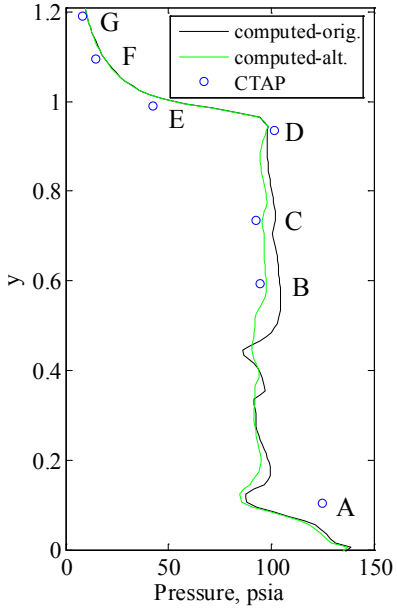

Figure 5.—Computed time-averaged, and measured CTAP pressures along the axis of the experimental RDE using the original and alternate area profiles.

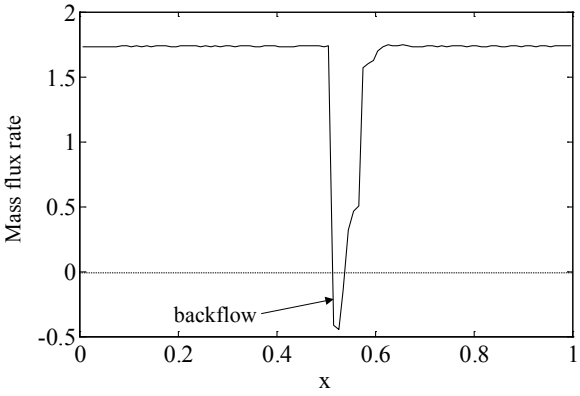

Figure 6.—Inlet mass flux profile as a function of circumferential distance for Test Point 1.

4.2 Test Point 2: Lean ($\phi = 0.42$)

As discussed earlier, the measurement of fuel and air flows (and thereby equivalence ratio, ϕ) in the experiment is done on a time-averaged basis. There are no diagnostics by which to ascertain the dynamic behavior through the injectors. As such, there is no way to know if the low equivalence ratio of this test point is achieved via the flow of a mixture at a uniform ϕ=0.42, or whether it may be achieved through pure air flowing over part of the cycle (i.e., purge flow) and the rest being a mixture closer to $\phi = 1.0$.

What is known is that the manifold pressure feeding the fuel is approximately 1/4 of that feeding the air. This suggests that as the high-pressure detonation passes a given point, the fuel flow is more likely to be interrupted (and for a longer fraction of the cycle) than the air. As such, the purge scenario just described is suspected to be active. This is bolstered by considering the known difficulty of sustaining detonations of lean hydrogen/air mixtures in devices at the scale of this experiment. Nevertheless, both the uniform ϕ and purge scenarios are considered below. For the purge scenario, it is assumed that whatever reactive mixture enters the device does so at $\phi = 1.0$. The remaining fluid entering is pure air ($\phi = 0.0$). The split between the two is adjusted by trial and error until the cycle averaged ϕ is equal to 0.42.

Figure 7 and Figure 8 show temperature contours for the two scenarios in a manner similar to Figure 1. Note that there are two detonation waves within the annular channel. The number of waves present cannot be predicted by this simulation since it is determined by physical details too fine to be captured under the present approach. As such, the number of waves is prescribed based on experimental observations. In Figure 8, the prescribed distribution of ϕ is shown at the bottom. The comparison with experiment of required inlet area and thrust for

each case is summarized in Table 2. As with Point 1, either scenario matches the experiment remarkably well.

The Test Point 2 pressure distributions for the two flow scenarios are shown in Figure 9. Again, the match with experiment is quite good. Discerning which of the two proposed flow scenarios is actually occurring in the experiment is not obvious given the data at hand. Additional instrumentation in subsequent experiments (e.g., high frequency ion gages, emission measurements) may provide answers.

4.3 Mixing Delay

The computational model assumes premixed fuel and air enters the RDE through the inlet, and allows a reaction to commence as soon as the fluid temperature exceeds a threshold value, T_{c0} (see Eq. (5)). As described earlier, the experimental fuel and air are injected separately and are likely to require some finite time (and associated convection distance) to mix before they will react. In order to cursorily examine the effect of this reaction delay, the simulation was modified such that a user specified number of computational cell rows near the inlet would not react, even if the threshold temperature was reached.

TABLE 2.—TEST POINT 2 COMPARISON

Scenario	$\varepsilon_{required}/\varepsilon_{actual} - 1$, %	$F_{computed}/F_{actual} - 1$, %
Uniform ϕ	–4	0
Purge	–3	–5

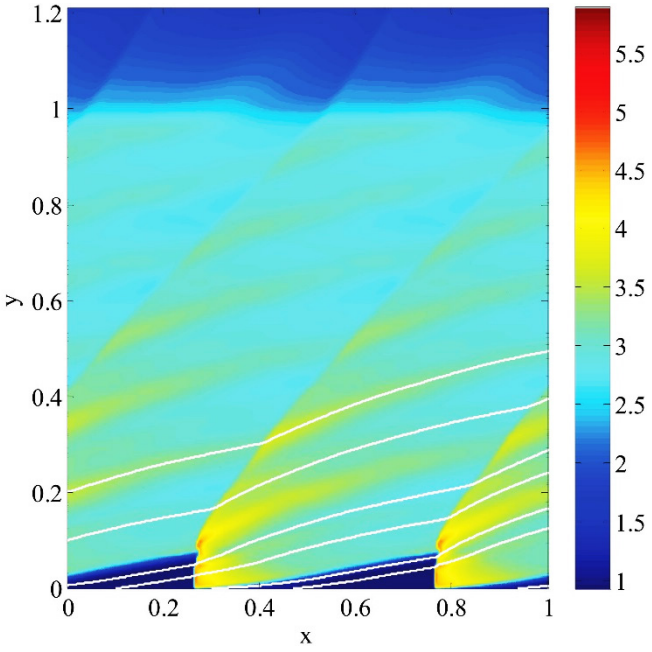

Figure 7.—Computed contours of temperature throughout the annulus of the experimental RDE, at the Point 2 flow conditions with uniform ϕ.

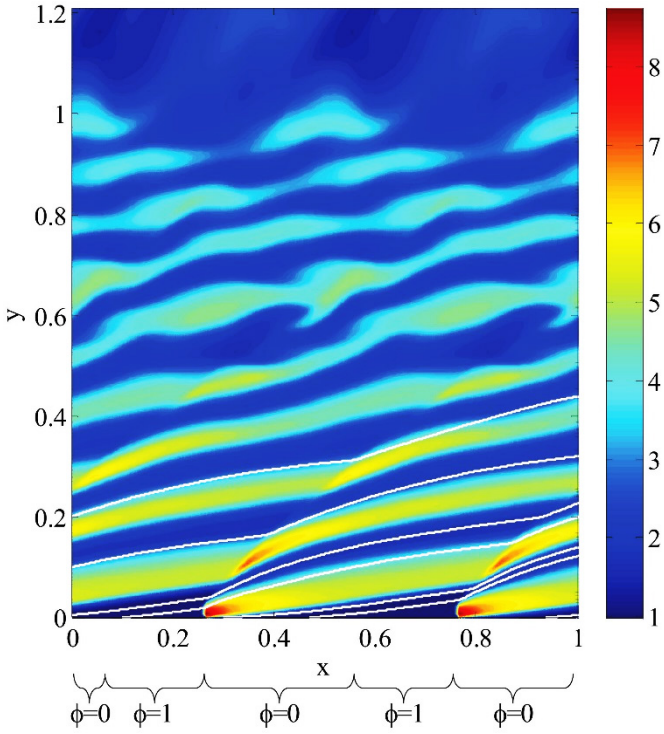

Figure 8.—Computed contours of temperature throughout the annulus of the experimental RDE, at the Point 2 flow conditions with purge.

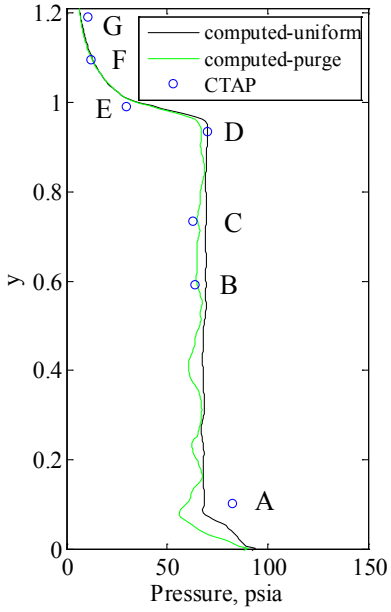

Figure 9.—Computed time-averaged, and measured CTAP pressures along the axis of the experimental RDE using the uniform ϕ and purge scenarios.

The results of applying this modification to the first 6 cell rows (i.e., $0 < y < 0.06$) for the Test Point 1 case are shown in Figure 10 and Figure 11 (similar to Figure 4 and Figure 5). As with other simulations, the value of ε required to match the mass flow rate was just 1 percent below the actual value. The computed gross thrust was only 1 percent below the measured value.

Comparing Figure 10 to Figure 4 it is seen that the detonation is shifted in the downstream direction. This results in a much better match between computed pressure and CTAP measurement near point A of Figure 11. As with other simplified sub-models presented in this paper, this result does not prove a mixing delay, but it does give it some measure of likelihood. It is also interesting to note (though it is not shown) that the shifting of the detonation reduces the backpressure on the inlet behind the detonation. This, in turn results in no predicted inlet backflow. No sensors were available in the experiment to validate this prediction.

5.0 Discussion

Favorable comparison between the present simulation and two test points from just one experiment does not constitute sufficient validation. More comparisons with varied experiments are necessary, and modification (as well as rejection) of the sub-models is inevitable. However, the results presented do suggest value in utilizing the code to examine the effect of various fluidic or geometric aspects on engine performance. This is something that is exceedingly difficult to do experimentally. For example, interrogating the Test Point 1 simulation reveals that 27 percent of the chemical energy is absorbed by the cold walls. The code can be run adiabatically (and inviscidly) to show that the heat transfer reduces gross thrust by 16 percent.

As a second example, the impact of deflagrated vs. detonated flow can be examined. It was mentioned earlier in the paper that the deflagration reaction rate parameter is variable, and that all of the simulations presented deflagrated approximately 8 percent of the incoming mixture. With the Test Point 1 simulation the reaction rate was adjusted so that approximately 17 percent of the mixture deflagrated. Doing so resulted in a 4 percent reduction in thrust.

Many other parametric variations could be considered with this simplified simulation approach. Doing so provides insights into both the physics of RDE operation, and possibilities for optimizing performance.

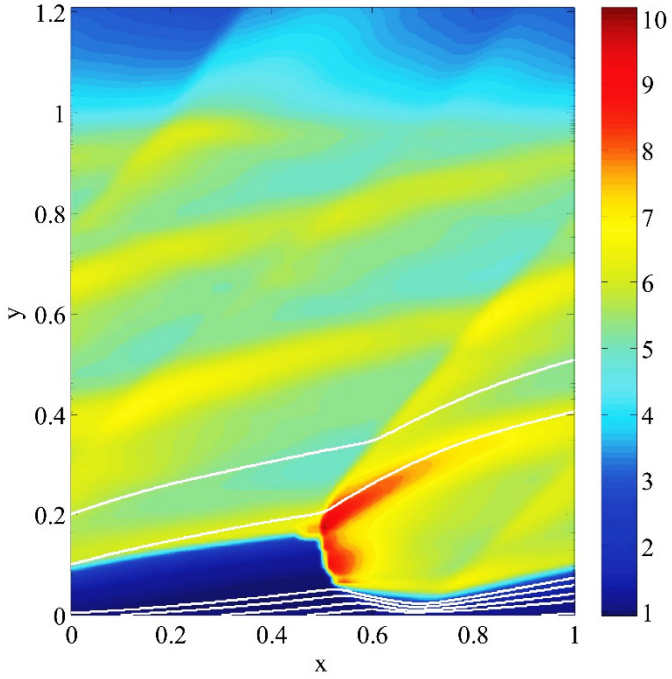

Figure 10.—Computed contours of temperature throughout the annulus of the experimental RDE at the Test Point 1 flow conditions with reaction delay.

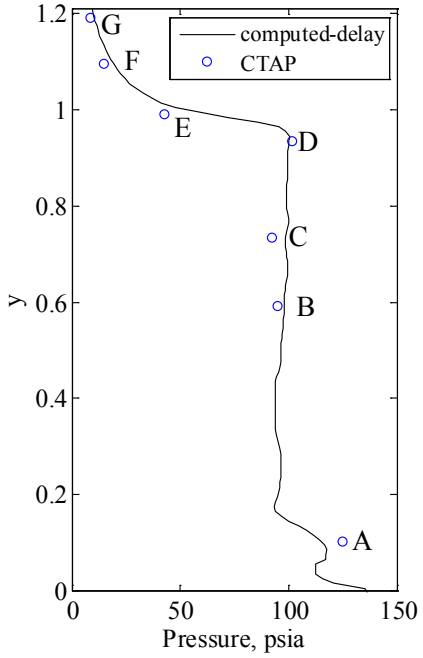

Figure 11.—Computed time-averaged, and measured CTAP pressures along the axis of the experimental RDE using reaction delay.

6.0 Conclusion

A quasi-two-dimensional, computational fluid dynamic (CFD) simulation of a rotating detonation engine (RDE) has been described. The computational approach is one of simplification, utilizing a relatively coarse grid, a single progress variable reaction mechanism, and operation in the detonation frame of reference. Real world effects such as those due to viscosity and heat transfer are added through the use of validated sub-models. The result is a rapidly converging simulation which provides steady-state solutions that capture the essential physics of an RDE. An experimental RDE was simulated and the output was compared with measurements at two operating points in terms of mass flow rate, thrust produced, and time-averaged pressure distributions. The comparison was shown to be favorable at both operating points. The utility of the code as a performance optimization tool and a diagnostic tool was illustrated by two example parametric variations. To the authors' knowledge, this represents the first publicly available direct comparison of simulated and measured RDE performance. Additional validation of the simulation is needed and planned.

References

1. Dyer, R., Naples, A., Kaemming, T., Hoke, J., Schauer, F., "Parametric Testing of a Unique Rotating Detonation Engine Design," AIAA 2012-121, Jan. 2012.
2. Naples, Hoke, J., Karnesky, J., Schauer, F., "Flowfield Characterization of a Rotating Detonation Engine," AIAA 2013-0278, Jan. 2013.
3. Sonwane, C., Claflin, S., Lynch, E., Stout, J., "Recent Advances in Power Cycles Using Rotating Detonation Engines with Subcritical and Supercritical CO2," SWRI 4th International Symposium - Supercritical CO2 Power Cycles, Pittsburgh, PA, Sep. 9-10, 2014.
4. Kato, Y., et al., "Thrust Measurement of Rotating Detonation Engine by Sled Test," AIAA 2014-4034, Jul. 2014.
5. Welsh, D.J., King, P.I., DeBarmore, N.D., Schauer, F.R., Hoke, J.L., "RDE Integration with T63 Turboshaft Engine Components, AIAA 2014-1316, Jan. 2014.
6. Paxson, D.E., "Numerical Analysis of a Rotating Detonation Engine in the Relative Reference Frame," AIAA-2014-0284, Jan. 2014, also NASA/TM—2014-216634, 2014.
7. Towery, C.A., et al., "Examination of Turbulent Flow Effects in Rotating Detonation Engines," AIAA 2014-3031, June 2014.
8. Schwer, D., Kailasanath, K., "Fluid Dynamics of Rotating Detonation Engines with Hydrogen and Hydrocarbon Fuels," Proceedings of the Combustion Institute, Vol. 34, No. 2, 2013, pp. 1991–1998.
9. Kim, T., Choi, J. "Numerical Study of Detonation Wave Propagation in 2-D Channels of Arbitrary Radius of Curvature," AIAA 2014-3903, Jul. 2014.
10. Paxson, D.E., "A General Numerical Model for Wave Rotor Analysis," NASA TM 105740, 1992.
11. Paxson, D.E., "An Improved Numerical Model for Wave Rotor Design and Analysis," AIAA-93-0482, Jan. 1993.
12. Perkins, H.D., et al., "An Assessment of Pulse Detonation Engine Performance Estimation Methods Based On Experimental Results," AIAA 2005-3831, July, 2005.
13. Paxson, D.E., Schauer, F.R., Hopper, D., "Performance Impact of Deflagration to Detonation Transition Enhancing Obstacles," AIAA-2009-0502, Jul. 2009, also, NASA/TM—2012-217629.
14. Rankin, B.A., Hoke, J.L., Schauer, F. R., "Periodic Exhaust Flow through a Converging-Diverging Nozzle Downstream of a Rotating Detonation Engine," AIAA 2014-1015, Jan. 2014.
15. White, F.M., Fluid Mechanics, McGraw-Hill, 1979, p. 381.
16. Paxson, D.E., Hoke, J.L., "Time Averaged Pressure Measurement in Fundamentally Unsteady Pressure Gain Combustion Systems," in Proc. JANNAF 45th Combustion Subcommittee, 33rd Airbreathing Propulsion Subcommittee, 27th Propulsion Systems Hazards Subcommittee, Monterey, CA, December, 2012, also NASA/TM—2013-217826, Jan. 2013.